J. Fluid Mech. (1986), *vol.* 169, *pp.* 409–428
Printed in Great Britain

Surface waves of large amplitude beneath an elastic sheet. Part 1. High-order series solution

By LAWRENCE K. FORBES†
Department of Mathematics, Kansas State University, Manhattan, KS 66506 USA

(Received 10 January 1985 and in revised form 26 February 1986)

Two-dimensional periodic waves beneath an elastic sheet resting on the surface of an infinitely deep fluid are investigated using a high-order series-expansion technique. The solution is found to have certain features in common with capillary–gravity waves; specifically, there is a countably infinite set of values of the flexural rigidity of the sheet at which the series solution fails, and these values are conjectured to be bifurcation points of the solution. Limiting waves of maximum height are found at each value of the flexural rigidity investigated. These are characterized by a cusp singularity in the elastic bending moment at the wave crest, and infinite fluid pressure there. For at least one value of the flexural rigidity, the series solution shows that the wave of maximum height also travels with infinite speed.

1. Introduction

The field of 'ice engineering' appears to be a rapidly growing area of scientific investigation, involving all aspects of ice growth on structures, damage to offshore constructions by floating ice sheets, and other problems having to do with facilities built upon the ice itself, and with the performance of icebreaking ships, for example. An important problem in this field would appear to be the accurate determination of the properties of waves travelling through water covered by a sheet of ice; such waves might, for example, be produced by a vehicle moving across the ice, and, if sufficiently large, could cause breaking of the ice sheet and consequent danger to the vehicle.

The present investigation stems from the observation of waves produced beneath a floating ice sheet by the periodic motion of a model icebreaking ship, during experiments performed in the large ice-room facility at the University of Iowa. These experiments are detailed in reports by Müller & Ettema (1984*a*, *b*). This study is aimed at determining the important characteristics of such waves.

The study of surface waves is one of the oldest problems in fluid mechanics, and the literature on the topic is vast. We do not presume to summarize this literature here, referring the reader instead to the review article by Schwartz & Fenton (1982). That the flow should be irrotational for an ideal fluid was first recognized by Stokes (1849), who later (Stokes 1880) developed the inverse formulation and Fourier-series solution technique that has formed the basis of several modern investigations. Schwartz (1974) automated Stokes' solution procedure, using a digital computer to evaluate the coefficients in Stokes' series, and obtained solutions of high accuracy

† Present address: Department of Mathematics, University of Queensland, St Lucia 4067, Queensland, Australia.

for waves of arbitrary height in fluid of arbitrary depth. His series solution has since been extended by Longuet-Higgins (1975), who discovered a remarkable maximum in the wave speed before the wave of maximum height is attained, and by Cokelet (1977).

Wilton (1915) applied Stokes' procedure to the problem of periodic surface waves in the presence of both gravity and surface tension, and demonstrated that the method yields solutions except at a countably infinite set of values of the surface tension, at which the series fails. He then showed that this failure of the series is associated with the existence of multiple solutions to the problem. Hogan (1980, 1981) has extended Wilton's series using a computer, in the manner described by Schwartz (1974), and Schwartz & Vanden Broeck (1979) computed numerical solutions to the problem, thus providing direct confirmation of the existence of multiple solutions.

Waves beneath a floating elastic plate appear to have been investigated first by Stoker (1957, p. 438). He was concerned with the transmission of waves beneath a floating breakwater, in the context of infinitesimal-wave theory. His work has since been extended by Evans & Davies (1968) to the case of three dimensions. Tuck (1982) has considered inviscid flow about a moving flexible sheet in extreme ground effect, obtaining a problem similar in some respects to Stoker's.

This paper concerns waves of arbitrary amplitude beneath an elastic sheet floating on the surface of an infinitely deep fluid. We follow Squire (1984) in assuming that this problem is capable of modelling ocean waves in the presence of sea ice when the fluid is incompressible and inviscid and flows irrotationally, and the ice behaves as an elastic plate. The experiments of Müller & Ettema (1984*a*, *b*) indicate that an ice sheet does indeed exhibit elastic behaviour under appropriate circumstances, and the equation derived in §2 allows for the possibilities that the curvature of the sheet may be large, and that the sheet may not necessarily be thin. In §3 periodic solutions are sought to the equations of motion, using Fourier series and perturbation expansions for the Fourier coefficients, and numerical results are presented in §4. The paper concludes in §5 with a discussion of the results and some suggestions for further research.

2. Formulation

We consider two-dimensional periodic waves of length λ moving with constant speed c from right to left in a fluid of infinite depth. An elastic sheet of thickness T and density ρ_{M} rests along the surface of the fluid. Consider a Cartesian coordinate system with the y-axis pointing vertically, moving with a wave crest; relative to these moving axes the waves are of permanent form, and the fluid moves from left to right in the direction of the positive x-axis. The peak-to-trough height of the waves is $2A$ and the acceleration due to gravity is g in the negative y-direction. The fluid is assumed to have density ρ.

An approximate equation describing the deflection of the elastic sheet will now be derived. From the classical theory of the bending of beams (see Donnell 1976) the bending moment M is related to the radius of curvature R of the beam by the equation

$$M = -\frac{D}{R}, \tag{2.1}$$

in which D is the flexural rigidity,

$$D = \frac{ET^3}{12(1-\nu^2)},$$

and E and ν are respectively Young's modulus and Poisson's ratio for the beam. The loading pressure P acting on the beam is then obtained in terms of the moment M from the equation

$$P-\rho_{\mathrm{M}} gT = -\frac{\mathrm{d}^2 M}{\mathrm{d}x^2}. \tag{2.2}$$

Dimensionless variables are now introduced, in which all lengths are scaled by the quantity $\lambda/2\pi$, and $(g\lambda/2\pi)^{\frac{1}{2}}$ is the corresponding reference velocity, following Schwartz & Vanden Broeck (1979). The moment M and pressure P are referred to $(\rho_{\mathrm{M}} g\lambda^3)(2\pi)^{-3}$ and $\rho g\lambda/2\pi$ respectively. Solutions to this problem are thus functions of five dimensionless parameters: The wave-speed number $\mu = 2\pi c^2/g\lambda$; the ratio $d_{\mathrm{M}} = \rho_{\mathrm{M}}/\rho$ of the densities of the sheet and the fluid; the dimensionless sheet thickness $H = 2\pi T/\lambda$; a coefficient $K = (16\pi^4 D)(\rho_{\mathrm{M}} g\lambda^4)^{-1}$ of flexural rigidity; and the half-wave height $\alpha = A/\lambda$. For later reference, we also define the wave steepness $\epsilon = \alpha/\pi$. In terms of these dimensionless variables, (2.1) and (2.2) become

$$M = -\frac{K}{R} \tag{2.3}$$

and

$$P-d_{\mathrm{M}} H = -d_{\mathrm{M}} \frac{\mathrm{d}^2 M}{\mathrm{d}x^2}. \tag{2.4}$$

The quantity R in (2.3) is the radius of curvature of the sheet at some point, measured from the *neutral plane*, which is approximately in the centre of the sheet, as shown in figure 1. Therefore

$$\frac{1}{R} = \frac{\mathrm{d}^2\eta/\mathrm{d}\xi^2}{(1+(\mathrm{d}\eta/\mathrm{d}\xi)^2)^{\frac{3}{2}}}, \tag{2.5}$$

where (ξ, η) are the coordinates of a point on the neutral surface. We wish to express (2.5) in terms of the coordinates (x, y) of a point on the lower surface of the sheet. From figure 1 it is clear that $\xi = R\cos\theta$ and $\eta = R\sin\theta$; in addition $x = (R-\frac{1}{2}H)\cos\theta$ and $y = (R-\frac{1}{2}H)\sin\theta$. The angle θ can be found from $\tan\theta = -(\mathrm{d}y/\mathrm{d}x)^{-1}$, and so

$$\left.\begin{aligned} \xi &= x - \frac{Hy'}{2(1+y'^2)^{\frac{1}{2}}}, \\ \eta &= y + \frac{H}{2(1+y'^2)^{\frac{1}{2}}}. \end{aligned}\right\} \tag{2.6}$$

After some algebra, (2.3), (2.5) and (2.6) may be combined to give

$$M = -\frac{Ky''}{(1+y'^2)^{\frac{3}{2}} - \frac{1}{2}Hy''}, \tag{2.7}$$

in which primes denote differentiation with respect to x.

It remains to state the equations governing the behaviour of the fluid beneath the elastic sheet. This fluid is assumed to be incompressible and inviscid and to flow without rotation; consequently, a velocity potential ϕ and stream function ψ exist, satisfying the Cauchy–Riemann equations

$$\left.\begin{aligned} u &= \phi_x = \psi_y, \\ v &= \phi_y = -\psi_x, \end{aligned}\right\} \tag{2.8}$$

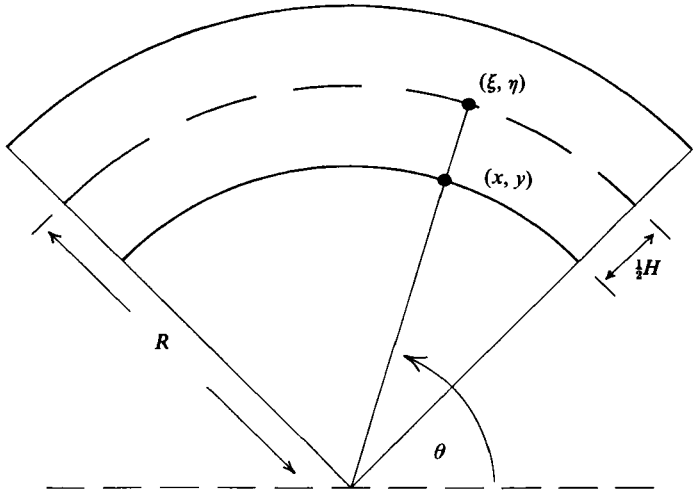

FIGURE 1. Definition sketch for the elastic sheet. The neutral plane is shown as a dashed line in the centre of the sheet.

in which u and v are respectively the horizontal and vertical components of fluid velocity. At infinite depth within the fluid,

$$u \to \mu^{\frac{1}{2}}, \quad v \to 0 \quad \text{as } y \to -\infty, \tag{2.9}$$

while the wave profile at the surface must satisfy

$$y(0) - y(\pi) = 2\alpha. \tag{2.10}$$

A representative wave cycle is sketched in figure 2. Following Tuck (1982), we assume that the pressure P in (2.4) can be equated to the pressure on the lower face of the elastic plate due to fluid forces; the latter is obtained from the Bernoulli equation

$$\tfrac{1}{2}(u^2+v^2)+y+P = \tfrac{1}{2}\mu + d_{\mathrm{M}} H. \tag{2.11}$$

Notice that the choice of Bernoulli constant in (2.11) forces the mean free-surface elevation

$$y_{\mathrm{av}} = \frac{1}{2\pi}\int_{-\pi}^{\pi} y \, \mathrm{d}x \tag{2.12}$$

to be zero in the absence of the elastic plate, as shown by Schwartz & Vanden Broeck (1979).

Equations (2.8) indicate that the complex potential $f = \phi + \mathrm{i}\psi$ is an analytic function of the variable $z = x + \mathrm{i}y$, in the entire fluid region. To simplify the formulation of the problem, the transformation of Stokes (1880) is invoked, in which f is now chosen as the independent variable and the solution sought in the form $z(f)$. Thus, although the location of the surface of the fluid is unknown in the physical z-plane, it maps simply to the line $\psi = 0$ in the f-plane. In addition, the lines $x = -\pi, 0, \pi$ map to lines $\phi = -\pi\mu^{\frac{1}{2}}, 0, \pi\mu^{\frac{1}{2}}$ respectively. Following Schwartz & Vanden Broeck (1979), a further conformal transformation

$$f = \mathrm{i}\mu^{\frac{1}{2}} \ln \zeta \tag{2.13}$$

is made to the f-plane, where $\zeta = r\mathrm{e}^{\mathrm{i}\theta}$. This has the effect of mapping each wave cycle in the f-plane into a closed disk of radius 1 in the ζ-plane, with the interface between the fluid and the elastic sheet, $\psi = 0$, mapping to the circle $r = 1$.

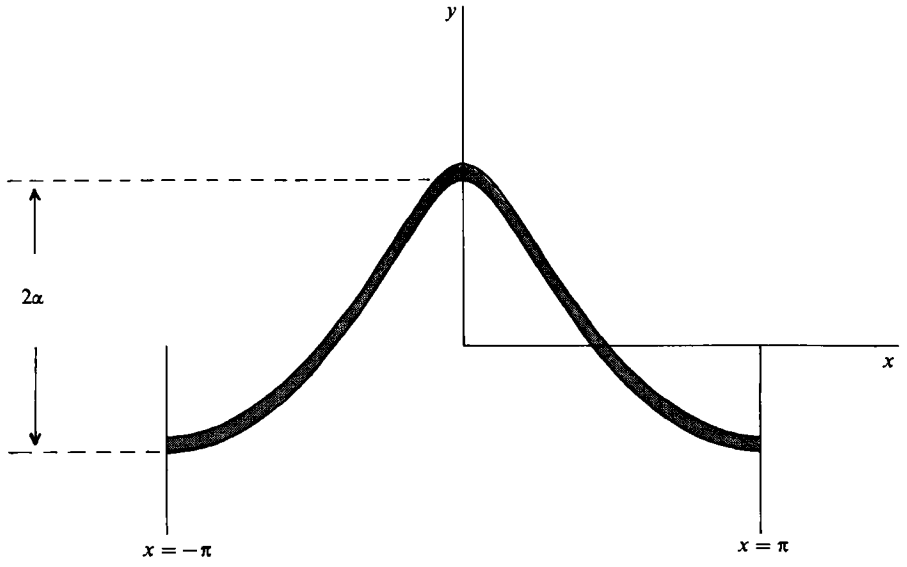

FIGURE 2. Sketch of a dimensionless wave profile, showing the peak–trough height 2α. The free-surface shape is taken from an actual solution for a pure gravity wave ($K = 0$).

The final form of the Bernoulli equation (2.11) in the ζ-plane is

$$\frac{\mu}{2}\left(\frac{1}{x_\theta^2+y_\theta^2}-1\right)+y+P = d_{\mathrm{M}} H \quad \text{on } r = 1, \tag{2.14}$$

where, from (2.4), the pressure is given by

$$P = d_{\mathrm{M}}\left[H-\frac{x_\theta M_{\theta\theta}-M_\theta x_{\theta\theta}}{x_\theta^3}\right] \quad \text{on } r = 1, \tag{2.15}$$

and (2.7) yields the moment M in the form

$$M = \frac{K(x_\theta y_{\theta\theta}-y_\theta x_{\theta\theta})}{(x_\theta^2+y_\theta^2)^{\frac{3}{2}}+\frac{1}{2}H(x_\theta y_{\theta\theta}-y_\theta x_{\theta\theta})} \quad \text{on } r = 1. \tag{2.16}$$

In the ζ-plane, (2.10) becomes

$$y(1,0)-y(1,\pi) = 2\alpha. \tag{2.17}$$

Thus we seek an analytic function $z(\zeta)$ in the disk $|\zeta| \leqslant 1$, satisfying conditions (2.14)–(2.17) on the boundary $r = 1$. The wave-speed parameter μ is also unknown, and is therefore to be sought as part of the solution.

3. The series solution

The solution $z(\zeta)$ to the equations of motion developed in §2 is sought in the Fourier-series form

$$z(\zeta) = \mathrm{i}\ln\zeta+\mathrm{i}\sum_{n=0}^{\infty} A_n\zeta^n, \tag{3.1}$$

in which the coefficients $A_n, n = 0, 1, 2, \ldots$ are all real. Equation (3.1) already satisfies the required periodicity conditions and the condition (2.9) at infinite depth, and so

it remains to choose the coefficients A_n and parameter μ to satisfy the surface conditions (2.14)–(2.17). Equation (2.17), for example, yields

$$\sum_{k=0}^{\infty} A_{2k+1} = \alpha. \tag{3.2}$$

The system of equations derived from (2.14)–(2.16) is too lengthy to be presented here in full, but may be obtained in a straightforward manner. To simplify the very substantial algebra involved, we have introduced seven intermediate products of series, at the surface $r = 1$, as follows:

$$\left.\begin{aligned} F^{(1)}(\theta) &= x_\theta^2 + y_\theta^2 \\ F^{(2)}(\theta) &= x_\theta y_{\theta\theta} - y_\theta x_{\theta\theta} \\ F^{(3)}(\theta) &= (x_\theta^2 + y_\theta^2)^{\frac{1}{2}} \\ F^{(4)}(\theta) &= (x_\theta^2 + y_\theta^2)^{\frac{3}{2}} \\ G^{(1)}(\theta) &= x_\theta^2 \\ G^{(2)}(\theta) &= x_\theta M_{\theta\theta} - M_\theta x_{\theta\theta} \\ G^{(3)}(\theta) &= x_\theta^3 \end{aligned}\right\} \quad \text{on } r = 1. \tag{3.3}$$

The intermediate variables in (3.3) and the quantities M and P are all developed as Fourier series. Thus

$$F^{(1)}(\theta) = \sum_{n=0}^{\infty} F_n^{(1)} \cos(n\theta), \tag{3.4}$$

with similar expressions for the other variables.

There thus results an infinite system of algebraic equations in the infinitely many unknowns $\mu, A_0, A_1, A_2, \ldots$. We seek the solution of this system using perturbation expansions in the half-wave height α, in the manner adopted by Schwartz (1974). We assume that

$$A_n = \beta^n \sum_{j=0}^{\infty} A_{nj} \beta^{2j}, \tag{3.5a}$$

$$F_n^{(1)} = \beta^n \sum_{j=0}^{\infty} F_{nj}^{(1)} \beta^{2j},$$

etc., and that

$$\mu = \sum_{j=0}^{\infty} \mu_j \beta^{2j}, \tag{3.5b}$$

where $\alpha = \beta S_c$, and S_c is a scale factor designed to prevent the coefficients A_{nj}, etc., from becoming excessively large. Values for S_c are typically in the range 0.1–0.5.

The linearized solution is obtained from (3.5) by retaining only first-order terms in β. To this order of approximation, we have

$$z(\zeta) = \mathrm{i} \ln \zeta + \mathrm{i}\alpha\zeta + O(\alpha^2), \tag{3.6a}$$

which yields the linearized free-surface profile

$$y(x) = \alpha \cos x + O(\alpha^2) \tag{3.6b}$$

and wave-speed number

$$\mu = 1 + d_M K + O(\alpha^2). \tag{3.6c}$$

An interesting situation arises as higher-order coefficients are computed in (3.5). For example, A_{20} is found to be

$$A_{20} = \frac{S_c^2[1-d_M K(\frac{13}{2}+H)]}{1-14d_M K},$$

which evidently is unbounded for $d_M K = \frac{1}{14}$. Similarly, A_{30} becomes infinite whenever $d_M K = \frac{1}{14}$ or $\frac{1}{39}$. The situation is clearly analogous to Wilton's (1915) original work on capillary–gravity waves, as the following theorem indicates.

Theorem

The series expansions (3.5) *fail* to yield solutions for A_{nj} and μ_j whenever

$$d_M K = \frac{1}{n(n^2+n+1)}, \quad n = 2, 3, 4, \ldots . \tag{3.7}$$

Proof

The proof of this result clearly consists of solving the very large system of recurrence relations resulting from (2.14)–(2.17), (3.1) and (3.3)–(3.5) for the coefficients A_{nj} and μ_j, and observing that these fail to be defined whenever (3.7) is satisfied. This has, of course, been done and is needed in the numerical work of the next section, but the general result is far too lengthy to be presented here. When $j = 0$, the equations can be solved separately, yielding the comparatively simple expression

$$A_{n0} = \tfrac{1}{2}(n-1)^{-1}[1-d_M K(n^2+n+1)\,n]^{-1}\Big[-n^2 d_M \sum_{s=1}^{n-1} M_{s0}(F^{(4)}_{n-s,0}+\tfrac{1}{2}HF^{(2)}_{n-s,0})$$
$$+d_M \sum_{s=1}^{n-1} s(n-s)(2s-n)\,M_{s0}\,A_{n-s,0}+\sum_{s=1}^{n-1} P_{s0}\,G^{(3)}_{n-s,0}+(A_{s0}+P_{s0})\,F^{(1)}_{n-s,0}\Big]. \tag{3.8}$$

Equation (3.8) cannot yield a solution for A_{n0} whenever (3.7) is satisfied, making the determination of A_{nj} and μ_j impossible. This confirms the theorem. □

The work of Wilton (1915), extended by Hogan (1981), and the numerical studies of Schwartz & Vanden Broeck (1979) indicate that, in the case of capillary–gravity waves, the failure of the series expansions (3.5) at discrete values of a surface-tension parameter is an indication that the problem possesses multiple solutions. We are likewise prepared to offer the following conjecture concerning the multiplicity of solutions to the present problem.

Conjecture

The values of K in (3.7) at which the series fails represent points at which bifurcation of the solution may occur. There are countably infinitely many families of solutions to this problem, and, as $K \to 0$, the number of them increases.

This conjecture can be confirmed analytically, in part, by demonstrating the existence of two solutions when $n = 2(d_M K = \frac{1}{14})$ in (3.7). This is done by generalizing the series (3.5) to allow terms of order α in the coefficient A_2 and in μ, as described by Wilton (1915) and Hogan (1981). This gives, for $d_M K = \frac{1}{14}$,

$$A_0 = -\tfrac{3}{4}\alpha^2 + O(\alpha^3),$$

$$A_1 = \alpha \mp \frac{9(5+2H)}{100}\alpha^2 + O(\alpha^3),$$

$$A_2 = \pm\tfrac{1}{2}\alpha + O(\alpha^2),$$

$$A_3 = \pm\frac{9(5+2H)}{100}\alpha^2 + O(\alpha^3),$$

$$A_4 = \left(\frac{45+16H}{210}\right)\alpha^2 + O(\alpha^3),$$

$$\mu = \frac{15}{14} \pm \left(\frac{15-2H}{28}\right)\alpha + O(\alpha^2).$$

The system of recurrence relations for A_{nj} and μ_j, of which (3.8) forms a part, has been programmed in FORTRAN on NAS 6630 and IBM 3083E digital computers, and solved to high order using double precision arithmetic. The series (3.5) are then summed using Padé approximants, as described by Schwartz (1974). This yields the coefficients $A_0, A_1, A_2, \ldots$ and the wave-speed parameter μ. Equation (3.1) then provides the solution at any desired point in the fluid.

It is now possible to draw wave profiles, by setting $\zeta = e^{i\theta}$ in (3.1). The pressure P and moment M in (2.15) and (2.16) are also available from the series solution, as is the mean free-surface elevation y_{av} in (2.12). In the ζ-plane this last quantity becomes

$$y_{av} = -\frac{1}{2\pi}\int_{-\pi}^{\pi} y(1,\theta)\, x_\theta(1,\theta)\, d\theta,$$

which, after the application of (3.1) and some algebra, finally yields

$$y_{av} = A_0 + \frac{1}{2}\sum_{n=1}^{\infty} nA_n^2. \tag{3.9}$$

The infinite sum in (3.9) is evaluated from the converged coefficients $A_0, A_1, A_2, \ldots$ using Padé approximants (rational fractions) as before. We have used the epsilon algorithm of Wynn (1966) to form the Padé fractions in every instance.

4. Presentation of results

When $K = 0$ in (2.14)–(2.16) the governing equations reduce to those describing pure gravity waves. The coefficients produced by our computer program in this case may then be checked against those given by Schwartz (1974) and Cokelet (1977) and are found to be in agreement with the results of these authors, confirming the correctness of our procedure, at least for $K = 0$. Two additional checks on the ability of the present method to compute gravity waves accurately are also available. The first of these is the condition (2.10), which is usually satisfied to at least eight decimal places, and the second is that $y_{av} = 0$ for the gravity wave, as explained in §2. Our solutions usually give y_{av} (computed from (3.9)) of the order of 10^{-10}.

In order to facilitate comparison with results to be presented for $K \neq 0$, we first show in figure 3 the difference $\mu - 1$ between the wave-speed parameter and the linearized value (given by (3.6*c*)) as a function of the half-wave height α, for the pure gravity wave ($K = 0$). As $\alpha \to 0$, $\mu - 1 \to 0$ as expected. For large α, however, the series solution indicates a local maximum for $\mu - 1$ *before* the theoretical maximum value $\alpha_{max} = 0.44353$ is reached. (This value of α_{max} is obtained from the result $\epsilon_{max} = 0.14118$ for maximum wave steepness, given by Schwartz (1974).) The existence of a local maximum in $\mu - 1$ was first observed by Longuet-Higgins (1975), and has been confirmed since by Cokelet (1977) and Hogan (1980).

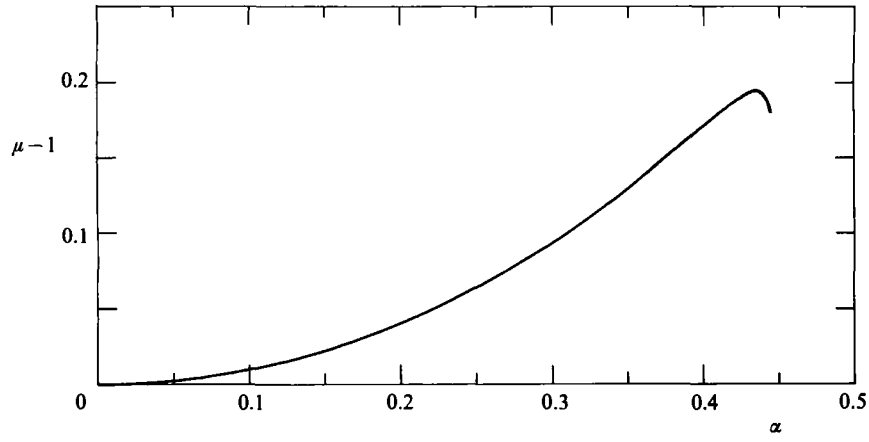

FIGURE 3. Wave-speed parameter as a function of α for the pure gravity wave.

Figure 4 shows three wave profiles for the case $K = 0.4, H = 0.005, d_{\mathrm{M}} = 0.9$ (and $S_{\mathrm{c}} = 0.3$), obtained at the three values of half-wave height $\alpha = 0.03, 0.075$ and 0.123. This value of $K = 0.4$ represents an elastic sheet of reasonable flexural strength. The Padé fractions used to sum the series (3.5a) for the Fourier coefficients did not converge with acceptable accuracy beyond $\alpha = 0.123$, and we conclude that the profile in figure 4 for this value of α represents the free-surface shape of a wave close to some maximum permissible height.

Unlike pure gravity waves, which are ultimately limited in height by the formation of a cusp singularity enclosing an angle of 120° at their crests, the waves in figure 4 do not display any such obvious singular behaviour. In order to understand the mechanism responsible for the failure of solutions to exist beyond about $\alpha = 0.123$, we present in figures 5(a) and (b) the moment M and pressure P for the three waves in figure 4 as functions of x. For $\alpha = 0.123$ figure 5(a) indicates that the moment has developed a remarkable, protruding, almost-cusped maximum at the crest $x = 0$. At this value of α, the pressure in figure 5(b) is observed to form a large peaked maximum at the wave crest.

A plausible explanation for the results in figures 4 and 5 may be formulated in the following manner. It appears from figure 5(a) that the wave of maximum height possesses a cusp singularity in its *bending moment* at the crest $x = 0$. We may model such behaviour by the function

$$M(x) \sim K(M_{\mathrm{c}} - C|x|) \quad \text{as } x \to 0, \tag{4.1}$$

where KM_{c} is the value of the moment at the crest. Now from (2.7) we have the approximate relation

$$M(x) \approx -Ky''(x)$$

at the free surface $y(x)$, which gives the surface elevation

$$y(x) \sim \tfrac{1}{6}C|x|^3 - \tfrac{1}{2}M_{\mathrm{c}}x^2 + y_{\mathrm{c}} \quad \text{as } x \to 0, \tag{4.2}$$

where y_{c} is the height at the crest. Note that the pressure in (2.4) involves the second derivative of the moment $M(x)$, which, from (4.1), yields

$$P(x) \sim d_{\mathrm{M}}H + 2Cd_{\mathrm{M}}K\delta(x) \quad \text{as } x \to 0, \tag{4.3}$$

in which $\delta(x)$ is the Dirac delta function. Thus waves are ultimately limited in height by the formation of a point of infinite pressure at the crest, as indicated by (4.3). Yet

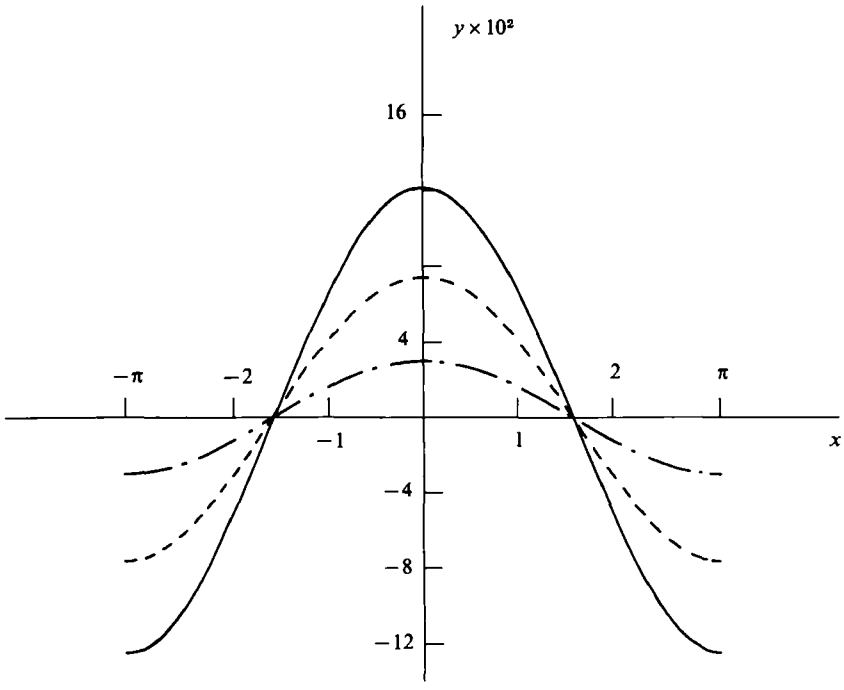

FIGURE 4. Wave profiles for $H = 0.005$, $K = 0.4$, $d_M = 0.9$ at the three half-wave heights $\alpha = 0.03$ (—·—), 0.075 (- - - -) and 0.123 (——).

(4.2) shows that the surface profile and its first two derivatives are continuous there, as is evidently the case in figure 4.

The difference between the wave-speed parameter μ and the linearized value, given by (3.6*c*), is shown as a function of α in figure 6. Unlike the case of the pure gravity wave (see figure 3), the speed now increases monotonically with α, apparently becoming infinite for the wave of maximum height. An analysis of the coefficients μ_j in (3.5*b*) using a Domb–Sykes plot (to be described later) indicates that μ becomes infinite at the approximate limiting value $\alpha_{\max} = 0.126$. We have attempted to study the approach to singular behaviour by reverting the series (3.5*b*) for the function $\mu(\beta^2)$, but the new function $\beta^2(\mu)$ provided little new information.

Figure 7 shows free-surface profiles for the case $H = 0.005$, $K = 0.05$, $d_M = 0.9$, at the three values of half-wave height $\alpha = 0.03$, 0.06 and 0.1. A Domb–Sykes plot reveals that $\alpha_{\max} \approx 0.107$, so that the case $\alpha = 0.1$ in figure 7 represents a surface profile of a wave very close to the maximum height. Note that the value $d_M K = 0.045$ lies between the first two critical values $\frac{1}{14}$ and $\frac{1}{39}$ given by (3.7), so that, according to the conjecture in §3, the waves in figure 7 are expected to represent a different branch of the solution from that shown in figures 4–6. However, the wave profiles in figure 7 seem very similar to those shown in figure 4 for the case $K = 0.4$, and to show the qualitative differences between these two branches of solution it is again necessary to examine the moment and pressure, which are shown for this case in figures 8(*a*) and (*b*) respectively.

It is clear that the moment again ultimately forms a cusp at the wave crest and that the pressure becomes large at this point, so that (4.1)–(4.3) again serve as a useful description of the approach to the wave of maximum height. However, figures 8(*a*, *b*)

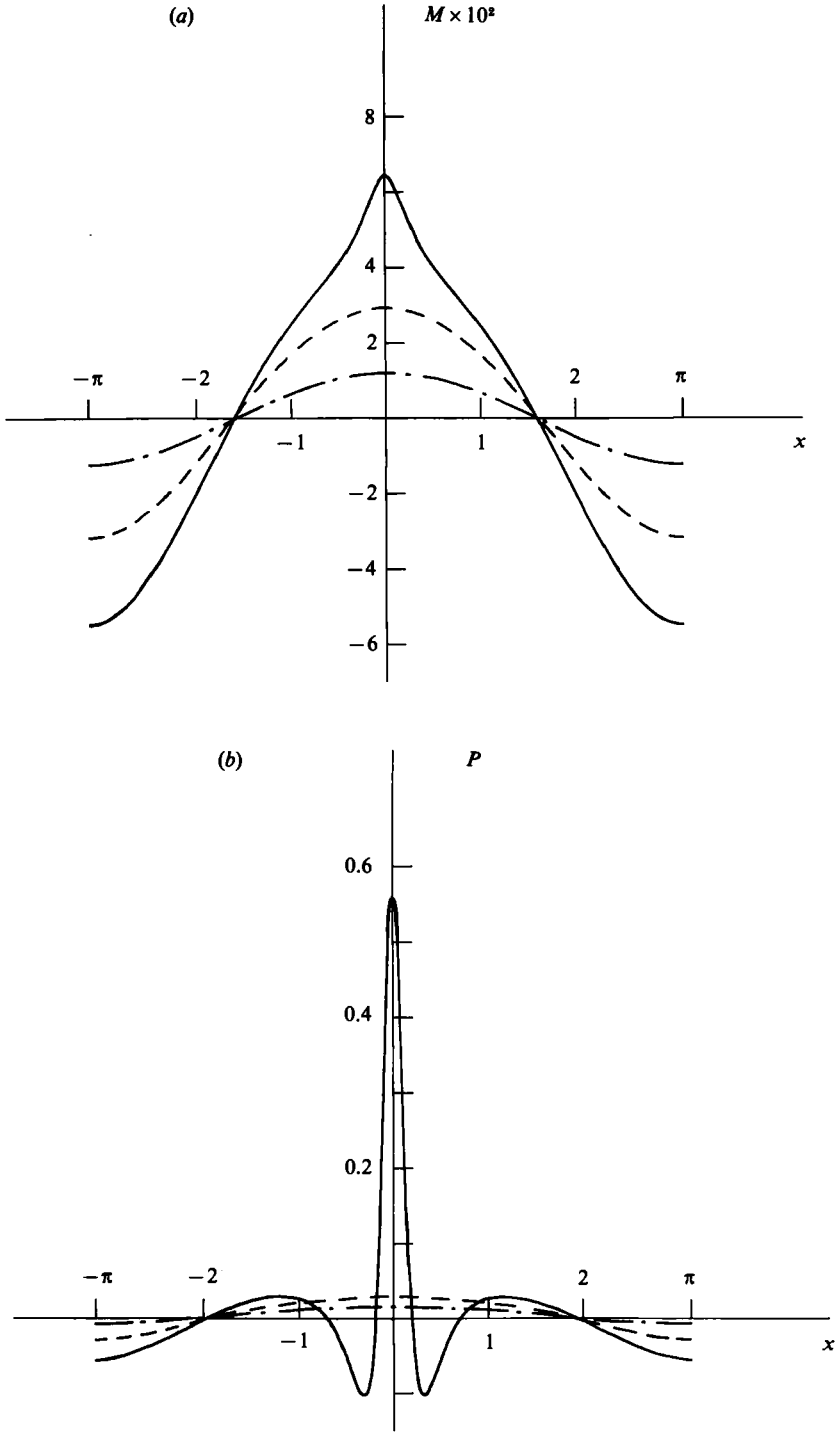

FIGURE 5. (*a*) Bending moment and (*b*) pressure profiles on the bottom face of the elastic sheet for $H = 0.005, K = 0.4, d_M = 0.9$ at $\alpha = 0.03$ (—·—), 0.075 (- - - - -) and 0.123 (——).

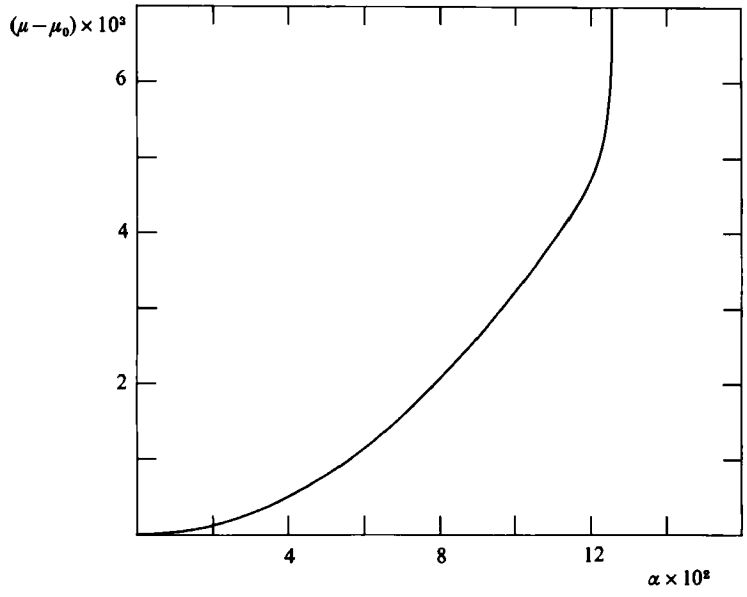

FIGURE 6. Wave-speed parameter as a function of α for $H = 0.005, K = 0.4, d_M = 0.9$.

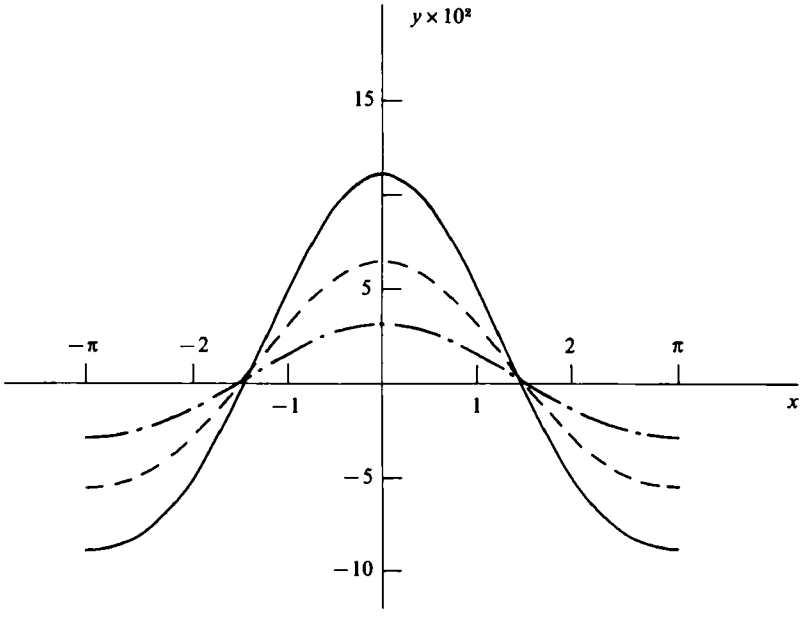

FIGURE 7. Wave profiles for $H = 0.005, K = 0.05, d_M = 0.9$ at the three half-wave heights $\alpha = 0.03$ (—·—), 0.06 (- - - -) and 0.1 (——).

for the case $K = 0.05$ differ from figures 5(a, b) ($K = 0.4$) by the presence of an additional dimple in both the moment and pressure profiles. This is similar to the situation existing in the case of capillary–gravity waves, as discovered by Wilton (1915), and discussed by Schwartz & Vanden Broeck (1979) and Hogan (1981), except that, for waves beneath an elastic sheet, these additional maxima and minima only

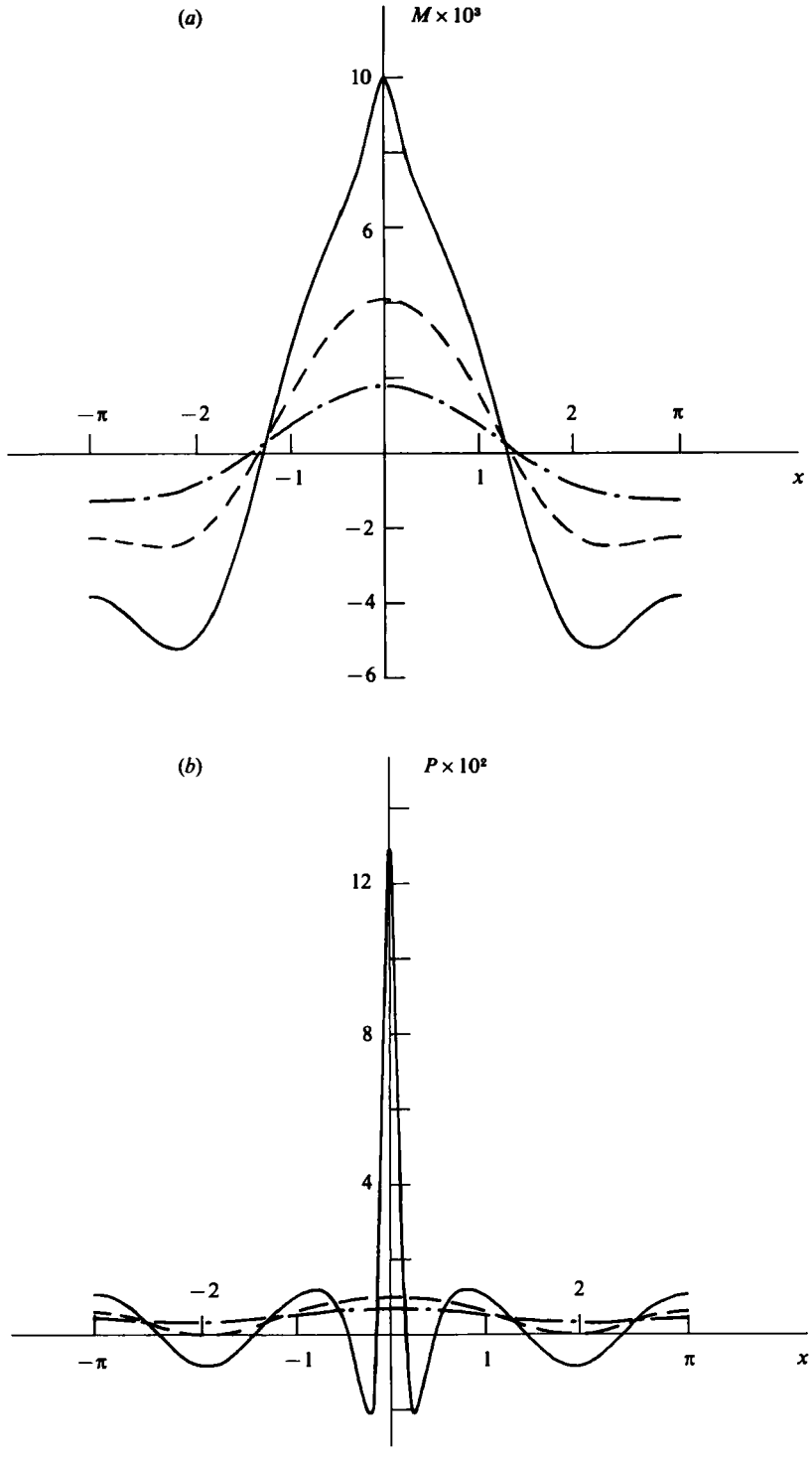

FIGURE 8. (*a*) Bending moment and (*b*) pressure profiles on the bottom face of the elastic sheet for $H = 0.005, K = 0.05, d_M = 0.9$ at $\alpha = 0.03$ (—·—), 0.06 (- - - -) and 0.1 (——).

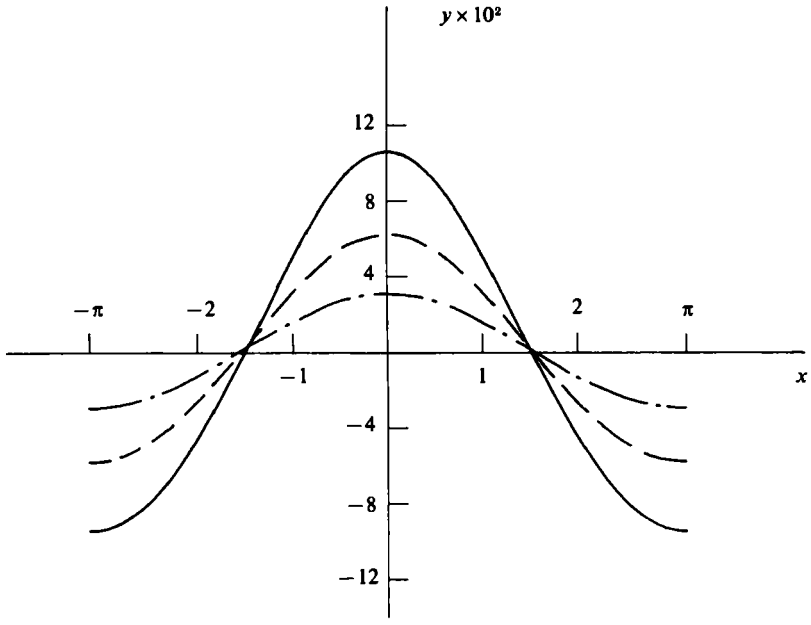

FIGURE 9. Wave profiles for $H = 0.005, K = 0.009, d_M = 0.9$ at the three half-wave heights $\alpha = 0.03$ (—·—), 0.06 (- - - - -) and 0.1 (——).

appear in the moment and pressure profiles, and evidently are not seen in the surface profile itself.

We show in figure 9 three solutions for the case $H = 0.005$, $K = 0.009$, $d_M = 0.9$, for half-wave heights $\alpha = 0.03, 0.06$ and 0.1. As will be demonstrated later, the profile for $\alpha = 0.1$ is almost that of the wave of maximum height. Although the waves in figure 9 ($K = 0.009$) represent a different branch of the solution to those shown in figure 7 ($K = 0.05$), according to the previous conjecture, there are only minor differences between the respective surface profiles, so that an examination of the moment and pressure is required to highlight qualitative differences between the solution branches.

Moment and pressure profiles are shown for this case ($K = 0.009$) in figures 10(a) and (b), and again it appears that the highest wave is characterized by a cusp of moment and a point of unbounded pressure at the crest. Notice that the cusp and pressure singularities now have the opposite sign to those in figures 5 and 8, however. In addition, the strengths of these singularities are very much reduced, which is modelled by allowing K to become small in (4.1) and (4.3). The pressure profile in figure 10(b), in particular, now possesses many secondary 'dimples'.

We now seek the radius of convergence of the series (3.5b) for μ in the case $H = 0.005$, $K = 0.009$, $d_M = 0.9$ shown in figures 9 and 10, attempting to determine the nature and location of the nearest singularity in the complex β^2 plane. For this purpose, a graphical extrapolation of the D'Alembert ratio test is employed, and is due to Domb & Sykes (1957). Suppose that the nearest singularity of the function $\mu(\beta^2)$ is of the form

$$\mu \to \begin{cases} C(\beta^2+\xi)^\delta, & \delta \neq 0, 1, 2, \ldots \\ C(\beta^2+\xi)^\delta \ln(\beta^2+\xi), & \delta = 0, 1, 2, \ldots \end{cases} \quad \text{as } \beta^2 \to -\xi, \tag{4.4}$$

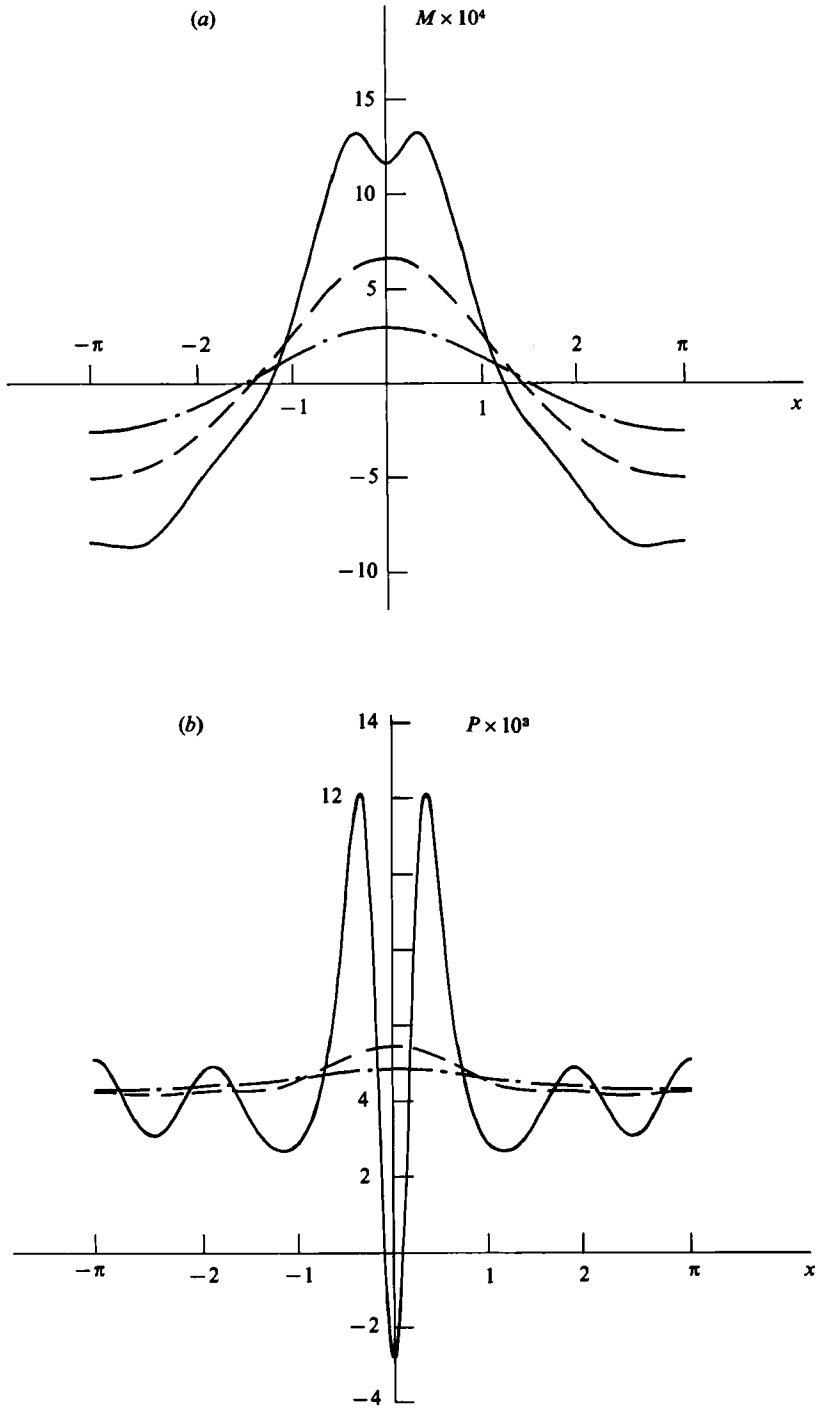

FIGURE 10. (*a*) Bending moment and (*b*) pressure profiles on the bottom face of the elastic sheet for $H = 0.005, K = 0.009, d_M = 0.9$ at $\alpha = 0.03$ (—·—), 0.06 (- - - -) and 0.1 (——).

where C, δ and ξ are constants. Then, from the binomial theorem, it follows that the coefficients μ_j in (3.5b) must satisfy the relation

$$\frac{\mu_j}{\mu_{j-1}} = \frac{1}{\xi}\left(-1+\frac{1+\delta}{j}\right) \tag{4.5}$$

as j becomes sufficiently large. Thus a graph of μ_j/μ_{j-1} against $1/j$ approaches a straight line with vertical intercept $-1/\xi$ and slope $(1+\delta)/\xi$. The maximum value of the half-wave height α for which the series (3.5b) converges is then $\alpha_{\max} = (-\xi S_c^2)^{\frac{1}{2}}$. Equation (4.5) shows that the parameters ξ and δ can be obtained from the limits

$$-\frac{1}{\xi} = \lim_{j\to\infty} \frac{\mu_j}{\mu_{j-1}} \tag{4.6a}$$

and

$$\delta = \lim_{j\to\infty} \xi j(j+1)\left[\frac{\mu_j}{\mu_{j-1}} - \frac{\mu_{j+1}}{\mu_j}\right] - 1, \tag{4.6b}$$

and these may be estimated using the extrapolative e_1 transformation due to Shanks (1955), for example.

A Domb–Sykes plot for μ in the case $H = 0.005$, $K = 0.009$, $d_M = 0.9$ is shown in figure 11. This graph is clearly asymptotic to a line of zero slope. For this case, the growth of round-off error in the coefficients μ_j seems unusually slow, and consequently it has been possible to show results to order $j = 60$ in figure 11. The Shanks transformation of the sequence of ratios μ_j/μ_{j-1} in (4.6a) converges to six figures, giving the value 2.24670 for the vertical intercept in figure 11. Since we have taken $S_c = 0.15$, this yields $\alpha_{\max} = 0.100073$, and the sequence (4.6b) for the singularity exponent then converges under the Shanks transformation to the value $\delta = -1.00$, correct to three figures. There thus seems little doubt that, at least for this case, the wave-speed parameter μ possesses a simple pole singularity on the positive real axis of α, of the form

$$\mu \to \frac{CK}{(\alpha-0.100073)(\alpha+0.100073)} \quad \text{as } \alpha \to \pm 0.100073, \tag{4.7}$$

where C is a constant.

The wave-speed parameter is shown as a function of α in figure 12, and evidently does exhibit singular behaviour near $\alpha = 0.1$. However, this value of the flexural rigidity ($K = 0.009$) is very small, so that the singularities (4.3) and (4.7) are quite difficult to detect. In addition, we have summed the series (3.5) using Padé fractions, which are capable of analytically continuing the solution in the complex α-plane right past the pole at $\alpha = \alpha_{\max}$, making detection of this weak singularity even more difficult. A portion of the curve in the physically meaningless region $\alpha > \alpha_{\max}$, obtained by the Padé fractions, is sketched with a dashed line in figure 12.

Thus far we have not considered the effect upon the solutions of changing the ice-sheet thickness H, which enters the problem in the inertial term $d_M H$ on the right-hand side of the Bernoulli equation (2.14), and also in (2.16), where it represents the fact that the radius of curvature of the sheet is measured from the neutral axis and not from the lower face of the ice sheet. The inertial term $d_M H$ merely accounts for the weight of the sheet, and, by (2.15), only influences the mean pressure, and cannot affect the wave profile itself. The effect of the thickness H in (2.16) upon the solutions is clearly more important, however, and a large number of computer programs have been run in order to quantify this effect. Nevertheless, the wave profiles and propagation speed are scarcely affected by moderate alterations to the value of H, and consequently the results do not warrant inclusion here.

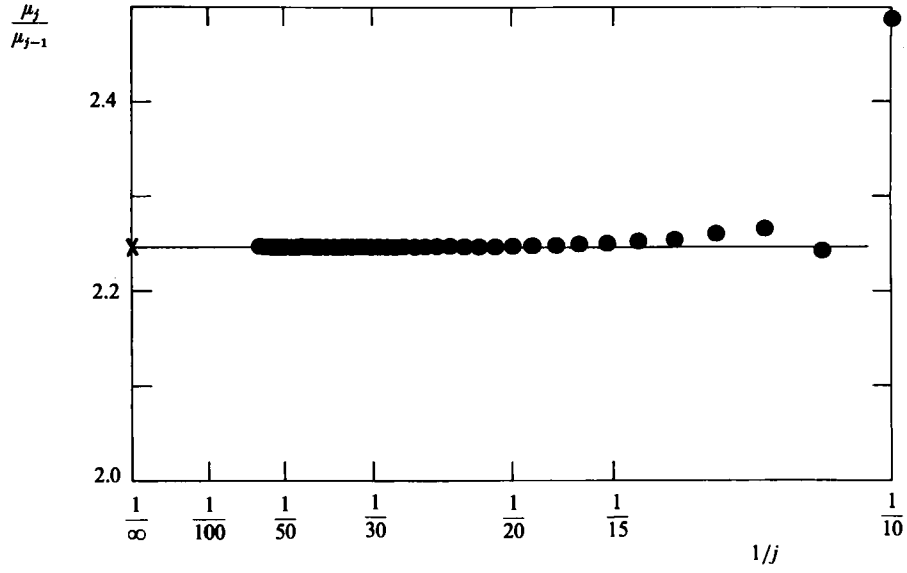

FIGURE 11. Domb–Sykes plot obtained from the series for the wave-speed parameter, for $H = 0.005, K = 0.009, d_{\mathrm{M}} = 0.9$.

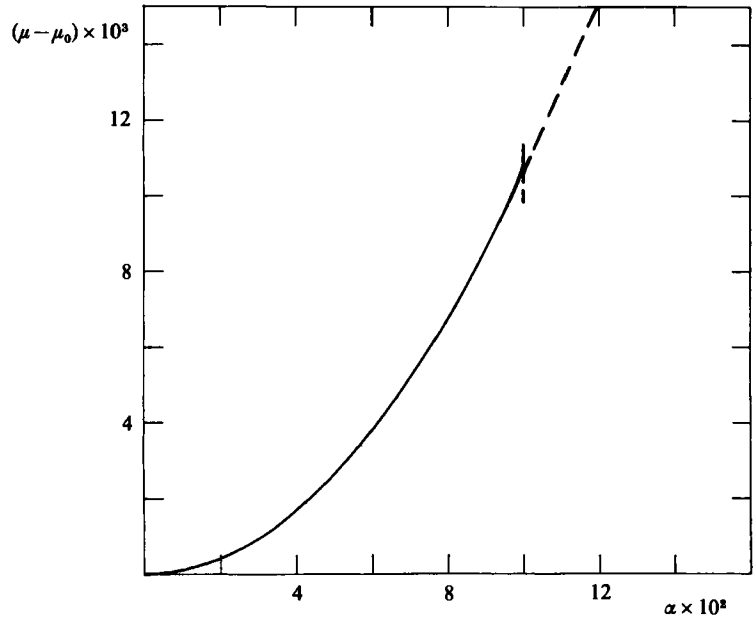

FIGURE 12. Wave-speed parameter as a function of α for $H = 0.005, K = 0.009, d_{\mathrm{M}} = 0.9$.

If the ice-sheet thickness H becomes very large, then it is clear from (2.14)–(2.16) that elastic effects become insignificant, and, since the Bernoulli equation (2.14) then becomes simply the equation describing pure gravity waves, these are the only possible outcome for very large H. Consequently, all the other branches of solution must vanish as H becomes large. We confirm that this is so in table 1, by showing the maximum permissible half-wave height $\alpha_{\max}$ for different values of H, in the case

H	$\alpha_{\max}$	δ
0.005	0.100073	−1.00
0.01	0.099968	−1.00
0.05	0.099137	−1.00
0.1	0.0981199	−1.00
1	0.0831670	−1.00
10	0.0348704	−1.01
50	0.010028	−1.00

TABLE 1. Maximum half-wave height and singularity exponent as functions of H, for the case $K = 0.009$, $d_M = 0.9$. The Shanks transformations of (4.6) converged in each case to the number of significant figures shown.

$K = 0.009$, $d_M = 0.9$. The quantities $\alpha_{\max}$ and the singularity exponent δ were obtained from Domb–Sykes plots by applying the Shanks e_1 transformation to the sequences defined in (4.6), and the results in table 1 indicate that $\alpha_{\max}$ indeed decreases as H increases, as expected. In addition it seems that in every case the limiting singularity remains a simple pole, of the type illustrated in (4.7).

5. Discussion

Periodic waves of arbitrary amplitude beneath an elastic sheet floating on the surface of an infinitely deep fluid have been investigated. Although we have ignored fluid viscosity, which would require that the no-slip condition be satisfied at the surface of the fluid, we do not anticipate serious errors arising from this omission, since our results indicate that the waves beneath the elastic sheet are of relatively small amplitude, and, unlike pure gravity waves, do not give rise to regions of extreme curvature. Consequently, viscous effects would be confined to a narrow boundary layer at the fluid surface, especially at large Reynolds numbers. The elastic sheet is assumed to behave as a classical beam of finite thickness, the curvature of which is not necessarily small. This problem differs conceptually from the gravity-wave case investigated by Schwartz (1974) and the capillary–gravity wave studies of Hogan (1980) in that our free-surface condition, while certainly nonlinear, nevertheless represents only an approximation to the real situation. However, we believe our surface condition to be adequate in almost every circumstance, and see few benefits at present in pursuing the higher-order elasticity theories, which are considerably more complicated than that adopted here.

The high-order series solution appears capable of convergence for all values of the flexural rigidity K, except the denumerably infinite set $d_M K = n^{-1}(n^2+n+1)^{-1}$, $n = 2, 3, 4, \ldots$. These singular values are conjectured to be associated with the existence of multiple solutions; this is confirmed in the case $n = 2$ in this paper, and could presumably be done at arbitrary K using a numerical method similar perhaps to that employed by Schwartz & Vanden Broeck (1979).

Results have been presented for several non-zero values of K. Each such result characterizes a different branch of the solution, evidenced by the different numbers of 'dimples' in the pressure profiles at large amplitude. The wave profiles are remarkably similar qualitatively, however. It has been determined that a maximum height exists for these waves, at which the bending moment and pressure at the crest become singular, and a simple mathematical description of these singularities has been given. The wave speed apparently becomes infinite at this maximum height;

this has been confirmed at least for one value of the flexural rigidity by means of a Domb–Sykes plot. It may prove possible in the future to develop a local solution, valid in some neighbourhood of the wave crest, which would define more clearly the nature of the singular behaviour of the highest wave as a function of K.

The infinite propagation speed predicted for the wave of maximum height is a result of the point of infinite pressure that is formed below the wave crest. In practice, the large pressure formed at the crest of a high wave is expected to result in cracking of the elastic sheet near this point, preventing the maximum-height wave of infinite propagation speed from ever being observable. For periodic waves beneath an elastic sheet, cracking would occur at uniform intervals, resulting in the formation of floating blocks of approximately equal length. This phenomenon is actually observed in the break-up of shore-fast ice, for example, as the photograph presented by Squire (1984) makes clear. In the context of ice engineering, such an event may well constitute a significant hazard, and we believe that an accurate table of the maximum theoretical wave height as a function of K, d_{M} and H could be of benefit to the ice-engineering community.

In this paper, we have not addressed the important question of the stability of the various branches of the solution. This difficult task is well beyond the scope of the present investigation, and is left to future research.

This work was undertaken in response to experiments conducted by Dr A. Müller of ETH, Zürich, and Dr R. Ettema of the Institute of Hydraulic Research, Iowa City, using the large ice-room facility at the University of Iowa. Subsequent assistance with the initial problem formulation by Mr M. Nagano of Mitsui Engineering and Shipbuilding Company, Tokyo, and discussion with Dr R. Ettema are gratefully acknowledged.

REFERENCES

COKELET, E. D. 1977 Steep gravity waves in water of arbitrary uniform depth. *Phil. Trans. R. Soc. Lond.* A **286**, 183–230.

DOMB, C. & SYKES, M. F. 1957 On the susceptibility of a ferromagnetic above the Curie point. *Proc. R. Soc. Lond.* A **240**, 214–228.

DONNELL, L. H. 1976 *Beams, Plates and Shells*. McGraw-Hill.

EVANS, D. V. & DAVIES, T. V. 1968 Wave–ice interaction. *Davidson Laboratory Report 1313, Stevens Institute of Technology, Hoboken, New Jersey.*

HOGAN, S. J. 1980 Some effects of surface tension on steep water waves. Part 2. *J. Fluid Mech.* **96**, 417–445.

HOGAN, S. J. 1981 Some effects of surface tension on steep water waves. Part 3. *J. Fluid Mech.* **110**, 381–410.

LONGUET-HIGGINS, M. S. 1975 Integral properties of periodic gravity waves of finite amplitude. *Proc. R. Soc. Lond.* A **342**, 157–174.

MÜLLER, A. & ETTEMA, R. 1984*a* Dynamic response of an ice-breaker hull to ice breaking. *Iowa Institute of Hydraulic Research Report IIHR273, The University of Iowa, Iowa City.*

MÜLLER, A. & ETTEMA, R. 1984*b* Dynamic response of an icebreaker hull to ice breaking. In *Proc. IAHR Ice Symp., Hamburg*, vol. II, pp. 287–296.

SCHWARTZ, L. W. 1974 Computer extension and analytic continuation of Stokes' expansion for gravity waves. *J. Fluid Mech.* **62**, 553–578.

SCHWARTZ, L. W. & FENTON, J. D. 1982 Strongly nonlinear waves. *Ann. Rev. Fluid Mech.* **14**, 39–60.

SCHWARTZ, L. W. & VANDEN BROECK, J.-M. 1979 Numerical solution of the exact equations for capillary–gravity waves. *J. Fluid Mech.* **95**, 119–139.

SHANKS, D. 1955 Non-linear transformation of divergent and slowly convergent sequences. *J. Maths & Phys.* **34**, 1–42.

SQUIRE, V. A. 1984 On the critical angle for ocean waves entering shore fast ice. *Cold Reg. Sci. Tech.* **10**, 59–68.

STOKER, J. J. 1957 *Water Waves.* Wiley-Interscience.

STOKES, G. G. 1849 On the theory of oscillatory waves. *Trans. Camb. Phil. Soc.* **8**, 441–455.

STOKES, G. G. 1880 In *Mathematical and Physical Papers*, vol. 1. Cambridge University Press.

TUCK, E. O. 1982 An inviscid theory for sliding flexible sheets. *J. Austral. Math. Soc.* B **23**, 403–415.

WILTON, J. R. 1915 On ripples. *Phil. Mag.* **29**, 688–700.

WYNN, P. 1966 On the convergence and stability of the epsilon algorithm. *SIAM J. Numer. Anal.* **3**, 91–121.